## Supplemental Material 1: Detailed description of experimental apparatus

The reactor (see Table 1) consists of a stainless steel chamber (volume 2350 $cm^3$) under high vacuum (a few times $10^{-8}$ Torr), with a central thermostatted copper finger to which both an optical window mount extending into the reactor and a liquid nitrogen Dewar open to the atmosphere are attached. An IR transparent window of silicon (0.78 $cm^2$ area) is inserted into the mount. A type T thermocouple is placed between the Si window and the body of the Cu window mount and a good thermal contact between Si and Cu is assured by a thin In foil. The signal from the thermocouple is processed through a homemade amplifier, with a gain of around 3500. It has been calibrated by measuring the water vapor pressure over pure ice in the range 170-220 K and compared to the values found in the literature (Marti and Mauersberger, 1993, Jancso and Pupezin, 1970). A key feature of the reactor is that the low temperature copper parts extending into the reactor are completely shielded from the gases which are admitted into the reactor chamber, such as HCl and water vapor, by a PTFE insulating cover. Moreover, in order to limit the interaction between the gases, especially HCl, and the reactor walls, the latter are heated and kept at 50°C. Therefore, once the system is cooled down, condensation of the admitted gases can only occur on the coldest point, namely the temperature-controlled Si substrate.

The film thickness is measured by applying HeNe laser interferometry at 632.8 nm. The solid phase is monitored by means of FTIR transmission spectroscopy employing a BIORAD FTS-575C spectrometer equipped with a cryogenic HgCdTe detector by typically collecting spectra averaging 4 scans at a resolution of 1 $cm^{-1}$. The two-chamber reactor is pumped to typically 10-8 Torr by a turbomolecular pump (VARIAN Turbo-300VHT, 250 l $s^{-1}$) attached to the lower (analysis) chamber, which is separated from the upper reactor part by a 6'' diameter gate valve. When the latter is closed, a calibrated leak or bypass valve shunting the reactor volume directly to the analysis chamber enables a stirred-flow regime of operation. A calibrated quadrupole mass spectrometer (Balzers Prisma QMS 200) housed in the lower chamber enables residual gas MS analysis of molecules evaporating from the solid phase deposited onto the Si support. A pressure gauge (MKS Baratron 220 AHS) with a 1 mbar full scale affords an absolute pressure measurement in the upper reactor chamber under either static or stirred-flow conditions. The system also includes an HCl injection line consisting of a Teflon coated glass calibrated volume of 60 $cm^3$ used as a reservoir for HCl vapor and monitored by a 2 Torr full scale absolute manometer (MKS Baratron). The inlet to the reactor is through a glass tube and a Swagelok micrometer dosing valve (Swagelok double pattern low-pressure metering valve with Vernier handle of type SS-SS2-D-TVVH). During the admission of HCl vapor in the reactor an upper limit to the flow rate of molecules injected can be found by measuring the pressure decrease in the calibrated volume as a function of time. The actual dose deposited onto the ice film may be lower than this measured value due to undesired interaction with the internal surface elements of the reactor. An additional, similar injection line is used to introduce bidistilled water vapor into the reactor. During the

injection, the pressure decrease in the 44 $cm^3$ reservoir can be measured using a 10 Torr full scale absolute manometer (MKS Baratron) and results in the measurement of the flow rate of molecules introduced into the chamber.

A number of tests have been carried out in order to confirm the presence of a unique cold spot in the reactor represented by the temperature-controlled Si window. Pure ice films have been grown and successively evaporated by simultaneously monitoring the MS signal for $H_2O$ (m/e 18) in comparison with the IR spectrum of the remaining film. In the earliest stages of experimental design and testing, when some parts of the cold copper cryostat were not completely insulated from the gas, the decrease in film thickness that was observed by the decrease in IR absorbance and by HeNe laser interferometric measurements, was not accompanied by a corresponding increase in the MS signal at m/e 18. In fact, part of the molecules that evaporated from the optical support recondensed on unidentified colder parts of the reactor internal surface, rather than being monitored before being pumped away. This was particularly evident when working under stirred-flow condition, that is at slow pumping speed. In addition, after the complete evaporation of the film from the optical window, a rise in the temperature caused an increase in the MS signal, due to the evaporation of the molecules that previously recondensed on some colder parts of the cryostat. Another clue for the presence of a cold spot was the disagreement between the measured number of molecules introduced into the reactor, calculated from the pressure decrease in the $H_2O$ calibrated volume, and the number of molecules actually deposited on the Si window, calculated from the absorbance at 3230 $cm^{-1}$ in the IR spectrum. When a cold spot was present, the number of molecules deposited onto the optical support was only less than half compared to the molecules introduced into the reactor. In contrast, when the cold spots were finally completely eliminated from the cryostat copper parts we obtained agreement within 20% between the three mass balance measurements, namely the admitted, deposited and evaporated molecules. The evaporation of the thin film of ice produced a simultaneous rise in the MS signal in contrast to the observed delay in case hot spots persisted. When the film was completely evaporated, the $H_2O$ MS signal rapidly decreased to background. Moreover, a further increase in temperature did not lead to an increase of the MS signal, as no more water was present in the reactor. The absence of cold spots in the SFR experimental set-up is the basis for obtaining quantitative results because it enables accurate calibration of the number of molecules deposited on the Si window, and thus the measurement of cross sections performed in the present work. A quantitative measurement of the $H_2O$ and HCl isotherms will be published shortly (Iannarelli et al., 2013).

## Supplemental Material 2: Supplemental Figures and Tables

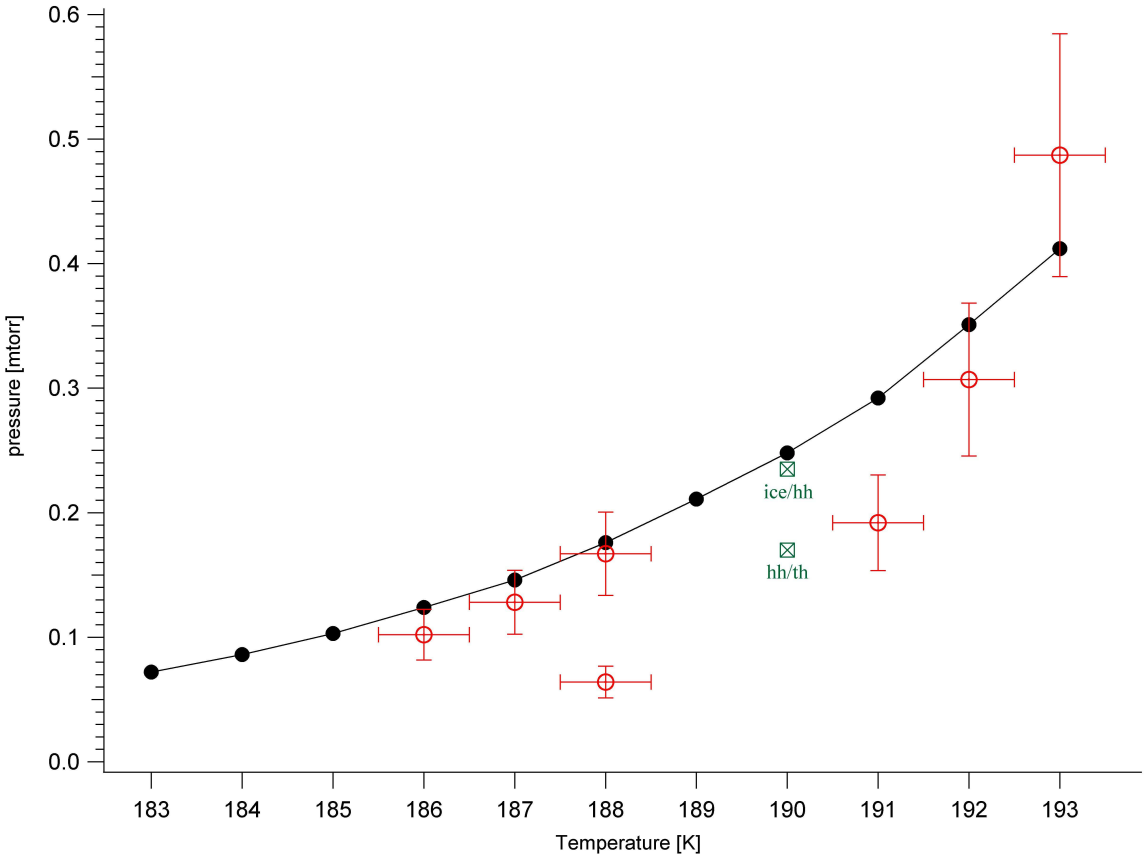


Figure A2.1. Equilibrium water vapor pressure over pure ice (circles, from Marti and Mauersberger, 1993, Jancso and Pupezin, 1970) compared to the measured equilibrium water vapor pressure over $HCl•6H_2O$ (squares) established under SFR conditions.

Table A2.1. Numerical values for $H_2O$ equilibrium vapor pressures displayed in Figure A2.1. ([a] is outlier, literature values from Hanson and Mauersberger, 1990)

| T/K | $P_{ss}$ (measured)/mTorr | $P_{eq}$ (correction factor 1.281)/ |
|---|---|---|
| 186 | 0.08 | 0.103 |
| 187 | 0.100 | 0.128 |
| 188 | 0.130 | 0.167 |
| 188[a] | 0.050 | 0.064 |
| 191 | 0.150 | 0.192 |
| 192 | 0.240 | 0.307 |
| 193 | 0.380 | 0.487 |
| 190 | Hexahydrate/Trihydrate Coexist. | 0.170 (lit) |
| 190 | Ice/Hexahydrate Coexistence | 0.235 (lit) |

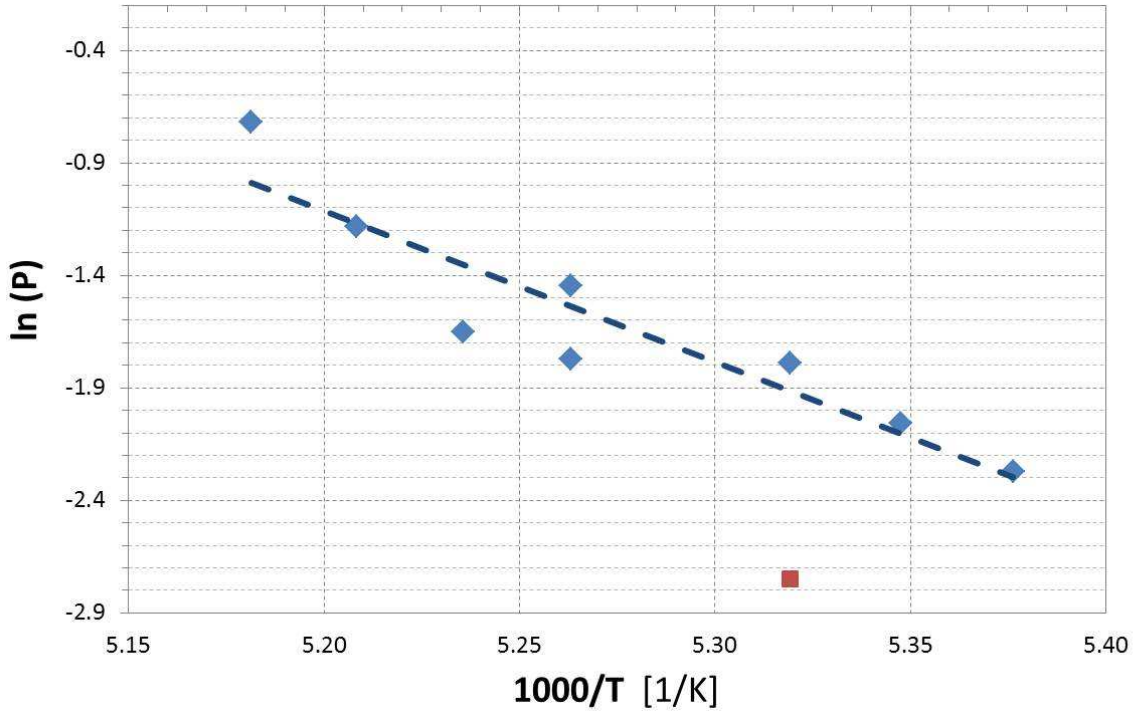


Figure A2.2. Van't Hoff plot of the $H_2O$ equilibrium pressure over pure HCl•$6H_2O$. From the slope of the fitted line (m = -6697.9) one obtains 55.7 ± 10.5 kJ $mol^{-1}$ for the enthalpy of reaction given in equation (13). The outlier (red square) has not been taken into account into regression.

Table A2.2. Absorbance of pure HCl hexahydrate samples at 3426 $cm^{-1}$ (Figure 3) as a function of the number of HCl•$6H_2O$ formula units present in the ice film.

| Sample number (symbol in Figure 3) | HCl•$6H_2O$ formula units | 2.303 $\log[I_0(\lambda)/I(\lambda)]$ [a] |
|---|---|---|
| 1 (circle) | 1.47 $10^{16}$ | 0.03 |
| 2 (octothorpe) | 1.50 $10^{16}$ | 0.032 |
| 3 (asterisk) | 2.09 $10^{16}$ | 0.041 |
| 4 (square) | 2.09 $10^{16}$ | 0.046 |
| 5 (triangle) | 2.99 $10^{16}$ | 0.069 |
| 1 | 3.63 $10^{16}$ | 0.078 |
| 2 | 3.63 $10^{16}$ | 0.083 |
| 4 | 4.27 $10^{16}$ | 0.088 |
| 6 (diamond) | 4.27 $10^{16}$ | 0.099 |
| 1 | 4.7 $10^{16}$ | 0.108 |

| | | |
|---|---|---|
| 5 | $5.13\ 10^{16}$ | 0.12 |
| 4 | $5.98\ 10^{16}$ | 0.127 |
| 3 | $5.98\ 10^{16}$ | 0.138 |
| 6 | $6.62\ 10^{16}$ | 0.147 |
| 1 | $6.84\ 10^{16}$ | 0.147 |
| 2 | $7.48\ 10^{16}$ | 0.157 |
| 4 | $8.12\ 10^{16}$ | 0.182 |
| 1 | $9.19\ 10^{16}$ | 0.214 |
| 6 | $1.22\ 10^{17}$ | 0.276 |
| 5 | $1.41\ 10^{17}$ | 0.318 |
| 3 | $1.58\ 10^{17}$ | 0.359 |
| 4 | $1.67\ 10^{17}$ | 0.38 |
| 6 | $1.77\ 10^{17}$ | 0.408 |
| 5 | $1.86\ 10^{17}$ | 0.438 |

[a] Absorbance *A* or optical density at $\lambda/cm^{-1}$ is defined as $A = \log[I_0(\lambda)/I(\lambda)]$.

Table A2.3. Temperature-pressure data for Figure 11 of selected experiments involving $HCl \cdot 6H_2O$ evaporation and decomposition to the amorphous $HCl/H_2O$ phase under SFR conditions.

| Phase/type of experiment | 1000/T ($K^{-1}$) | P(HCl)/Torr |
|---|---|---|
| HH/decomposition | 5.63 | $8.50\ 10^{-8}$ |
| | 5.27 | $2.20\ 10^{-7}$ |
| amorphous/decomposition | 5.24 | $2.50\ 10^{-7}$ |
| | 5.02 | $4.50\ 10^{-7}$ |
| HH/decomposition | 5.6 | $1.80\ 10^{-7}$ |
| | 5.27 | $4.50\ 10^{-7}$ |
| amorphous/decomposition | 5.23 | $5.30\ 10^{-7}$ |

| | | |
|---|---|---|
| | 4.8 | $1.50\ 10^{-6}$ |
| HH/decomposition | 5.54 | $2.60\ 10^{-7}$ |
| | 5.25 | $7.90\ 10^{-7}$ |
| amorphous/decomposition | 5.21 | $8.80\ 10^{-7}$ |
| | 4.98 | $1.80\ 10^{-6}$ |
| HH/evaporation | 5.71 | $1.26\ 10^{-6}$ |
| | 5.62 | $1.34\ 10^{-6}$ |
| | 5.56 | $1.37\ 10^{-6}$ |
| | 5.49 | $1.52\ 10^{-6}$ |
| | 5.43 | $1.68\ 10^{-6}$ |
| | 5.38 | $1.88\ 10^{-6}$ |
| | 5.35 | $2.00\ 10^{-6}$ |
| | 5.38 | $1.98\ 10^{-6}$ |
| | 5.35 | $2.05\ 10^{-6}$ |
| HH/evaporation | 5.65 | $4.80\ 10^{-7}$ |
| | 5.43 | $6.70\ 10^{-7}$ |
| HH/evaporation | 5.75 | $5.97\ 10^{-7}$ |
| | 5.52 | $9.62\ 10^{-7}$ |
| | 5.43 | $1.15\ 10^{-6}$ |
| | 5.35 | $1.43\ 10^{-6}$ |
| | 5.32 | $1.55\ 10^{-6}$ |
| | 5.29 | $1.95\ 10^{-6}$ |
| | 5.21 | $2.92\ 10^{-6}$ |
| HH/evaporation | 5.71 | $8.50\ 10^{-7}$ |
| | 5.62 | $9.10\ 10^{-7}$ |
| | 5.56 | $1.09\ 10^{-6}$ |
| | 5.52 | $1.20\ 10^{-6}$ |
| | 5.56 | $1.07\ 10^{-6}$ |

## Supplemental Material 3: Molecular Monolayer of HCl adsorbed on $H_2O$ ice.

A point of contention in the $HCl/H_2O$ phase diagram at low temperatures is the notion of a molecular monolayer of HCl on top of the ice film at saturation because most experiments do not provide any information on the thickness of the disordered region that is more reactive compared to the core non-disordered region of the "ice" existence area. A consensus value of (2-3) x $10^{14}$ molecule $cm^{-2}$ at 200 K seems to prevail, with some values being significantly larger. Flückiger et al. (1998, Figure 10) obtain 3.1 x $10^{14}$ at 185 K for the disordered phase (purple point in Figure 12) for vapor-deposited ice. Others obtain (2.0 ± 0.7) x $10^{14}$ in the range 215 to 230 K (Hynes et al., 2001), (1.1 ± 0.6) x $10^{14}$ at 201 K (Lee et al., 1999), 2.5 x $10^{14}$ at 208 K (Abbatt et al., 1997), 2.3 x $10^{14}$ at 180 K increasing to 2.7 x $10^{14}$ at 200 K (Henson et al., 2004). However, larger values for the HCl coverage are sometimes obtained on some vapor-deposited ice samples. Examples are 5 x $10^{14}$ at 200 K (Hanson et al., 1992), 1.0 x $10^{15}$ at 200 K (Abbatt et al., 1992) and (7.3 ± 1.6) x $10^{15}$ at 183 K (Foster et al., 1997). This shows that temperature, morphology and HCl partial pressure may have an influence on the saturation coverage of HCl on ice without going into any detail. However, vapor-deposited ice is certainly the most atmospherically relevant substrate despite some disparate results on the saturation coverage. Therefore, a thorough characterization and knowledge of the substrate is important when comparing results from different laboratories.